Optics Letters

Controllable double-helical microstructures by photonic orbital angular momentum for chiroptical response

Jincheng Ni,[1,2] Yanlei Hu,[1,4] Shunli Liu,[1] Zhaoxin Lao,[1] Shengyun Ji,[1] Deng Pan,[1] Chenchu Zhang,[3] Bing Xu,[1] Jiawen Li,[1] Dong Wu,[1,*] and Jiaru Chu[1]

[1]CAS Key Laboratory of Mechanical Behavior and Design of Materials, Department of Precision Machinery and Precision Instrumentation, University of Science and Technology of China, Hefei, Anhui 230027, China
[2]Department of Electrical and Computer Engineering, National University of Singapore, Singapore 117583, Singapore
[3]Institute of Industry and Equipment Technology, Hefei University of Technology, Hefei, Anhui 230009, China
[4]e-mail: huyl@ustc.edu.cn
*Corresponding author: dongwu@ustc.edu.cn

Received 15 January 2021; revised 16 February 2021; accepted 18 February 2021; posted 19 February 2021 (Doc. ID 419798); published 11 March 2021

Three-dimensional helical microstructures are abundant in nature and can be applied as chiral metamaterials for advanced nanophotonics. Here we report a flexible method to fabricate double-helical microstructures with single exposure by recording the chirality of incident optical vortices. Two coaxial optical vortices can interfere to generate a helical optical field, confirmed by the numerical simulation. The diameters of double-helical microstructures can be tailored by the magnitude of topological charges. This fast manufacturing strategy provides the opportunity to efficiently yield helical microstructures. Finally, the chirality of double-helical microstructures can be reversibly read by optical vortices, demonstrating a strong chiroptical response.

https://doi.org/10.1364/OL.419798

Chiral objects, which cannot be superimposed on its mirror image by simple rotations or translations, are ubiquitous in nature such as hands, amino acids, proteins, seashells, and helical towers [1,2]. Apart from natural organisms, chiral micro/nanostructures fabricated by top-down or bottom-up methods also exhibit extraordinary optical properties and are widely used in advanced photonic devices. Typically, circular dichroism (CD) is used for characterizing the optical activity of materials, exhibiting different complex refractive indices for left- and right-handed polarization states. Due to the weak dichroism selection of planar-chiral structures, chiral structures have been extended along the third dimension to maximize the interaction with light such as stacking planar metamaterials with twist [3] and helical structures [4]. In this regard, femtosecond-laser two-photon polymerization represents a simple and high-precision method for fabricating three-dimensional (3D) microstructures [5,6] and photonic crystals [7]. For example, single-helical metamaterials by direct laser writing can be considered as circular polarizers [8]. Moreover, triple-helical microstructures by a stimulated emission depletion (STED)-inspired laser lithography method can generate a broadband CD in the mid-infrared range [9]. Nevertheless, given that it is time-consuming for a point-by-point scanning method [10–13], high-efficiency micro/nanofabrication methods for helical structures with tunable parameters remain to be realized.

Vortex beams with helical phase wavefronts $e^{il\varphi}$ intrinsically have photonic orbital angular momentum (OAM) [14–16]. The donut-shaped vortex beams have been comprehensively used in optical communications [17,18], STED fluorescence microscopy [19], optical tweezers [20], and micro/nanofabrication [21,22]. In addition, the chirality of optical vortex can also be transferred into materials by chiral light–matter interaction such as relief patterns on an azobenzene-containing polymer film [23] and chiral structures in isotropic polymers [24]. However, the characteristic parameters of vortex-dependent chiral structures are still non-tunable.

Here we propose a flexible and rapid strategy to fabricate double-helical microstructures by superimposing two optical vortices with different topological charges. The chiral microstructures are realized by a single exposure of spatial-phase-modulated vortex beam. The coaxial optical vortices can interfere to generate a double-helical optical field under a high-numerical-aperture (NA) objective lens. Moreover, the chirality of double-helical microstructures can be probed by optical vortices, which shows a strong chiroptical response.

The detailed fabrication procedure of double-helical microstructures is illustrated in Fig. 1(a). A linearly polarized femtosecond-laser pulse with a central wavelength of 800 nm is modulated by a spatial light modulator (SLM) for achieving double-helical microstructures. A $4f$ system consisting of two convex lenses is used to filter undesired diffraction of the modulated vortex beams. Then the modulated light beam is focused by a 60× oil-immersion objective lens into a polymer

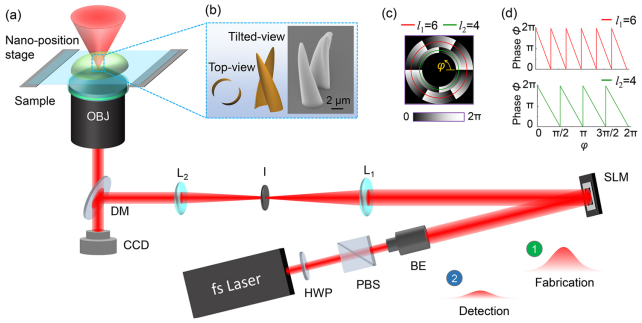

Fig. 1. Experimental setup and conceptual design of the holograms for fabricating and detecting double-helical microstructures. (a) Schematic of the optical setup. The femtosecond laser is modulated by an SLM to generate a structured optical field. After illuminating in the photoresist, a double-helical microstructure is achieved. HWP, half-wave plate; PBS, polarizing beam splitter; BE, beam expander; L, lens; CCD, charge-coupled device; DM, dichroic mirror. (b) Schematic and tilted-view scanning electron microscope (SEM) image of the double-helical microstructure. (c) Phase mask displayed on the SLM consists of two optical vortices with topological charges $l_1 = 6$ and $l_2 = 4$. (d) Phase value Φ of two optical vortices as a function of the azimuthal coordinate φ.

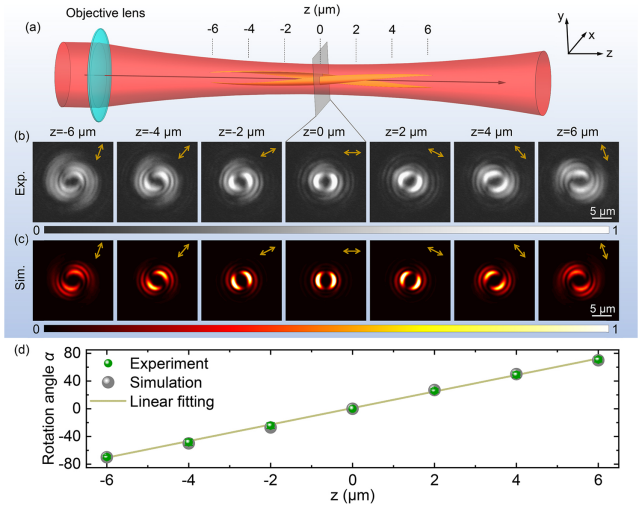

Fig. 2. Generation of 3D helical optical fields by vortex beams. (a) Schematic of the modulated vortex beam focused by a high-NA objective lens. (b) Experimental and (c) simulated optical fields at different transversal plane in 2 μm steps along the z axis. The orientations of two-petal profiles are indicated by orange arrows. (d) Rotation angle α of helical optical fields with respect to the horizontal line as a function of the z position.

sample SZ2080 (see Supplement 1 for details). Finally, double-helical microstructures are achieved with an exposure time of 100 ms and laser energy of 5 mJ [Fig. 1(b)]. The OAM beams can be conveniently generated by modulating a Gaussian beam with the SLM, which is loaded with an optimized pitchfork hologram. Two petal-shaped intensity profiles are obtained by the interference of two optical vortices with topological charge $l_1 = 6$ and $l_2 = 4$. For realizing the interference between two optical vortices, the hologram displayed on the SLM consists of two spiral phase profiles, as shown in Fig. 1(c). The two concentric spiral phase regions can modulate the Gaussian beam into two optical vortices with topological charges $l_1 = 6$ and $l_2 = 4$, respectively. The annular hologram can be presented as

$$\emptyset(r, \varphi) = \begin{cases} (l_1 * \varphi) \bmod 2\pi & 360 < r \le 540 \\ (l_2 * \varphi) \bmod 2\pi & 270 < r \le 360 \\ 0 & \text{else} \end{cases}, \quad \textbf{(1)}$$

where r is the radial pixels from the center of the hologram, and φ is the azimuthal angle. In Fig. 1(d), we plot the phase value Φ as a function of azimuthal angle φ in two phase regions with $l_1 = 6$ and $l_2 = 4$, respectively.

Owing to the tight focus of the high-NA (NA = 1.35) objective lens, the two concentric optical vortices can interfere to generate an optical helical field, as depicted in Fig. 2(a). The transversal intensity distribution can be captured by a CCD camera. Due to the remnant OAMs of superimposed optical vortices, the spatial rotation of optical spiral fields can be observed along the z axis in experiments and simulations [Figs. 2(b) and 2(c)]. The simulated optical field under a high-NA objective lens is calculated by the vectorial Debye diffraction theory (see Supplement 1 for details). The measured intensity distributions are in good agreement with the simulations, which indicates that the OAM beams produced in our experiment are of very high quality. Figure 2(d) exhibits the measured rotation angle of an optical helical field defined as

$$\alpha = A\Delta z, \quad \textbf{(2)}$$

where α is the rotation angle, $A = 11.66°/\mu m$ is the rotation rate, and Δz is the propagating distance. The rotation rate A is dependent on the topological charges and microscope objective, implying that the helical angle of the generated optical field is tunable. As a result, the double-petal profiles propagate in a twist trajectory with respect to the z axis.

After precisely controlling the laser power and exposure time, only the central fraction of the optical field is larger than the polymerized energy threshold and can be recorded in the photoresist [25]. The handedness of double-helical microstructures can be flexibly controlled by adjusting the holograms. Left-handed double-helical microstructures are achieved after being exposed under superimposed optical vortices with topological charges $l_1 = 6$ and $l_2 = 4$ [Fig. 3(a)]. Figure 3(b) shows the two petal-shaped profiles on the transversal plane at $z = 2$ μm, where an obvious rotation of the optical field can be observed. The optical field maintains rotation along the propagating direction, which is induced by an azimuthal phase gradient. More details about azimuthal intensity and phase are shown in Fig. 3(c). The calculated phase distribution has six multiples of 2π around the azimuth. In contrast, the right-handed double helicoids can be obtained by superimposed optical vortices with topological charges $l_1 = -6$ and $l_2 = -4$, as shown in Fig. 3(d). The intensity and phase distributions of superimposed vortices are mirror-symmetric for opposite topological charges [Figs. 3(e) and 3(f)]. By precisely controlling the sites with a nano-positioning stage, a large-area array of double-helical microstructures up to 1 mm^2 can be conveniently achieved in 5 min, compared to more than 2 h by the conventional single-point scanning method (see Supplement 1 for details). Intriguingly, the number of bright petals on the optical fields is relative to the value of $\Delta l = |l_1 - l_2|$. Therefore, triple-helical microstructures can also be realized by superimposed optical vortices with topological charges $l_1 = 6$ and $l_2 = 3$ (see Supplement 1 for details).

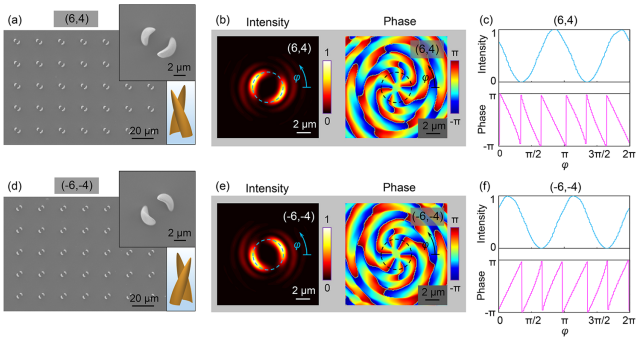

Fig. 3. Experimental fabrication and theoretical analysis of double-helical microstructures with opposite handedness. (a) SEM image of a large-area array of double-helical microstructures fabricated by two optical vortices with topological charges $l_1 = 6$ and $l_2 = 4$. The inset is a magnified image. (b) Simulated intensity distribution (left panel) and phase profile (right panel) on the transversal plane at $z = 2$ μm. (c) Azimuthal distribution of the intensity and phase obtained in (b). (d)–(f) Double-helical microstructures with right handedness corresponding to (a)–(c) fabricated by two optical vortices with topological charges $l_1 = -6$ and $l_2 = -4$.

By varying topological charges l_1 and maintaining the relationship of $l_2 = l_1 - 2$, the optical fields with different diameters are realized, as shown in Figs. 4(a) and 4(b). The cross-sectional intensity distribution of two petal-shaped profiles is shown in Figs. 4(c) and 4(d). After interfering two optical vortices, the diameter of superimposed optical vortices is between the small and large diameters. As a result, the diameters of superimposing optical vortices can be tunable for varying topological charges l_1 and l_2. The diameter of the double-helical microstructure is linearly increased (from 3.3 to 6.7 μm) by varying the value of l_1 from 4 to 8 [Fig. 4(e)]. The larger axial extent of the helical microstructure can also be realized by adjusting the optical setup and fabrication parameters [26]. However, when the helical microstructures are fabricated with a relative higher height, the tips of two petals can touch each other to assemble as a helicoid induced by capillary force (see Supplement 1 for details).

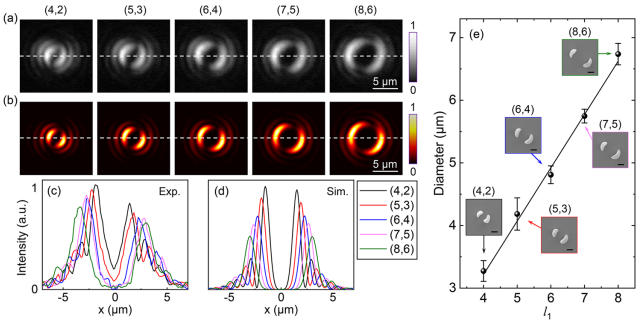

Fig. 4. Controllable diameters of double-helical microstructures with different topological charges. (a) Measured and (b) simulated intensity distributions by varying vortex beams with topological charges $\Delta l = l_1 - l_2 = 2$. (c),(d) Cross-sectional intensity distributions of the experimental and simulated results, respectively. (e) Measured diameter D of double-helical microstructures as a function of topological charge l_1. The solid line represents the theoretical diameters for different topological charge l_1. The insets are the corresponding SEM images of double-helical microstructures. Scale bars, 2 μm.

Beyond recording the chirality of optical vortices by polymerized double-helical microstructures, the conserved chirality can also be observed by optical vortices reversibly. To detect the chiroptical properties of double-helical microstructures, we measured the chiroptical spectra of a pair of typical microhelicoids with the same diameter ($D = 4.8$ μm) but opposite handedness, as shown in Fig. 5(a). The asymmetric reflectance can be obtained by illuminating optical vortices on the double-helical microstructures with the same optical setup [Figs. 5(b) and 5(c)]. Consequently, the chiroptical properties of double-helical microstructures can be achieved by measuring vortical dichroism (VD) value as

$$\mathrm{VD} = 2 \times (I_R - I_L) / (I_R + I_L) \times 100\%, \quad (3)$$

where I_R and I_L are the reflection intensity of double-helical microstructures under right-handed wavefront (RHW) and left-handed wavefront (LHW) illumination, respectively. Our measurements show that VD responses are different for left- and right-handed helical microstructures, indicating chiroptical selectivity. We can obtain a strong VD value (~ 40%) at topological charge $|l| = 10$ by matching the dimensions of vortex beams and microstructures [see Fig. 5(d)]. The VD spectra of helicoids with opposite handedness are mirror-symmetric with respect to the zero line. The VD spectra of double-helical

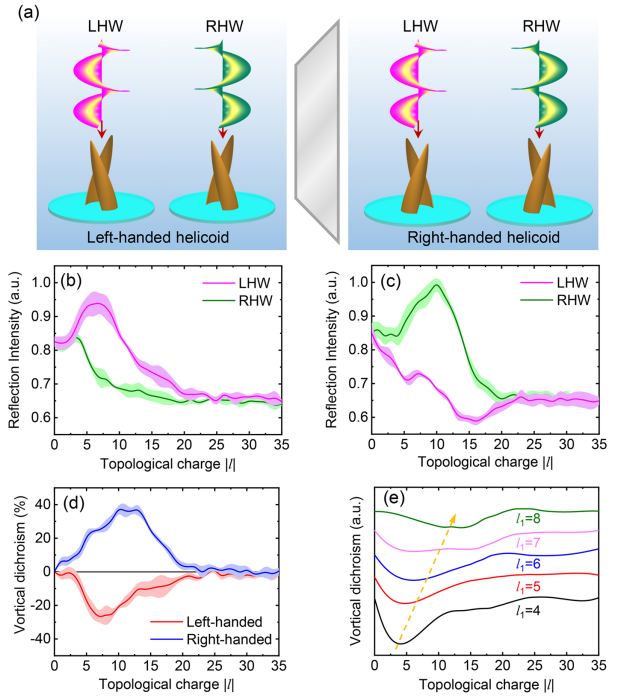

Fig. 5. Chiroptical detection of double-helical microstructures. (a) Schematic of OAM beams with LHW or RHW impinging on left- (left panel) and right-handed (right panel) double-helical microstructures, respectively. (b),(c) Measured reflection intensity on (b) left- and (c) right-handed helicoids ($D = 4.8$ μm) illuminated by optical vortices with different topological charges $|l|$. (d) Measured optical VD on left- and right-handed microstructures versus topological charge $|l|$. (e) VD spectra of the left-handed microstructures with different diameters fabricated by varying topological charges. The arrow indicates the double-helical microstructures fabricated by topological charge l_1 ranging from 4 to 8. Each solid line shows the mean value, and the shading indicates the standard deviation of multiple measurements.

microstructures with larger diameters have a right shift due to the dimensional matching, as shown in Fig. 5(e). Therefore, according to the VD spectra, the recorded information about chirality of structured optical vortices can also be read reversibly by vortex beams at the wavelength of 800 nm.

In summary, an efficient and flexible method is reported for generating double-helical microstructures using a spatially modulated femtosecond-laser beam. The double-helical optical field under a high-NA objective lens is generated by interfering two optical vortices with different topological charges. The generation mechanism is investigated by experimentally measuring the 3D field distribution, agrees well with the theoretical simulations. The transversal petals and chirality of helical microstructures are dependent on the OAM difference of optical vortices. The diameters of microstructures can be further adjusted by the magnitude of their topological charges. Finally, we observe giant VD signals on the double-helical microstructures. This Letter provides a powerful illustration that helical microstructures by single-exposure modulated beams offer strong optical properties effects with applications in chiroptical spectroscopy and chiral optics.

Funding. Major Science and Technology Projects in Anhui Province (201903a05020005); National Key Research and Development Program of China (2017YFB1104303, 2018YFB1105400); Fundamental Research Funds for the Central Universities (WK2090000016, WK2090050048, YD2090002005); National Natural Science Foundation of China (51805509, 51875544, 52075516, 61927814, 91963127).

Acknowledgment. The authors are grateful to the USTC Center for Micro and Nanoscale Research and Fabrication.

Disclosures. The authors declare no conflicts of interest.

Supplemental document. See Supplement 1 for supporting content.

REFERENCES

1. M. Hentschel, M. Schaferling, X. Y. Duan, H. Giessen, and N. Liu, Sci. Adv. **3**, e1602735 (2017).
2. L. Dordevic, F. Arcudi, A. D'Urso, M. Cacioppo, N. Micali, T. Burgi, R. Purrello, and M. Prato, Nat. Commun. **9**, 3442 (2018).
3. Y. Zhao, M. A. Belkin, and A. Alu, Nat. Commun. **3**, 870 (2012).
4. J. C. Ni, C. W. Wang, C. C. Zhang, Y. L. Hu, L. Yang, Z. X. Lao, B. Xu, J. W. Li, D. Wu, and J. R. Chu, Light Sci. Appl. **6**, e17011 (2017).
5. D. Wu, J. Xu, L. G. Niu, S. Z. Wu, K. Midorikawa, and K. Sugioka, Light Sci. Appl. **4**, e228 (2015).
6. Z. X. Lao, Y. L. Hu, D. Pan, R. Y. Wang, C. C. Zhang, J. C. Ni, B. Xu, J. W. Li, D. Wu, and J. R. Chu, Small **13**, 1603957 (2017).
7. K. K. Seet, V. Mizeikis, S. Matsuo, S. Juodkazis, and H. Misawa, Adv. Mater. **17**, 541 (2005).
8. J. K. Gansel, M. Thiel, M. S. Rill, M. Decker, K. Bade, V. Saile, G. von Freymann, S. Linden, and M. Wegener, Science **325**, 1513 (2009).
9. J. Kaschke and M. Wegener, Opt. Lett. **40**, 3986 (2015).
10. Z. X. Lao, Y. L. Hu, C. C. Zhang, L. Yang, J. W. Li, J. R. Chu, and D. Wu, ACS Nano **9**, 12060 (2015).
11. L. Yang, A. El-Tamer, U. Hinze, J. W. Li, Y. L. Hu, W. H. Huang, J. R. Chu, and B. N. Chichkov, Appl. Phys. Lett. **105**, 041110 (2014).
12. X. Q. Liu, Q. D. Chen, K. M. Guan, Z. C. Ma, Y. H. Yu, Q. K. Li, Z. N. Tian, and H. B. Sun, Laser Photonics Rev. **11**, 1770032 (2017).
13. Y. L. Sun, Q. Li, S. M. Sun, J. C. Huang, B. Y. Zheng, Q. D. Chen, Z. Z. Shao, and H. B. Sun, Nat. Commun. **6**, 8612 (2015).
14. L. Allen, M. W. Beijersbergen, R. J. C. Spreeuw, and J. P. Woerdman, Phys. Rev. A **45**, 8185 (1992).
15. M. Padgett, J. Courtial, and L. Allen, Phys. Today **57**, 35 (2004).
16. S. Franke-Arnold, L. Allen, and M. Padgett, Laser Photonics Rev. **2**, 299 (2008).
17. N. Bozinovic, Y. Yue, Y. X. Ren, M. Tur, P. Kristensen, H. Huang, A. E. Willner, and S. Ramachandran, Science **340**, 1545 (2013).
18. S. T. Mei, M. Q. Mehmood, S. Hussain, K. Huang, X. H. Ling, S. Y. Siew, H. Liu, J. H. Teng, A. Danner, and C. W. Qiu, Adv. Funct. Mater. **26**, 5255 (2016).
19. K. I. Willig, S. O. Rizzoli, V. Westphal, R. Jahn, and S. W. Hell, Nature **440**, 935 (2006).
20. J. E. Curtis and D. G. Grier, Opt. Lett. **28**, 872 (2003).
21. K. Toyoda, K. Miyamoto, N. Aoki, R. Morita, and T. Omatsu, Nano Lett. **12**, 3645 (2012).
22. J. C. Ni, Z. Y. Wang, Z. Q. Li, Z. X. Lao, Y. L. Hu, S. Y. Ji, B. Xu, C. C. Zhang, J. W. Li, D. Wu, and J. R. Chu, Adv. Funct. Mater. **27**, 1701939 (2017).
23. A. Ambrosio, L. Marrucci, F. Borbone, A. Roviello, and P. Maddalena, Nat. Commun. **3**, 989 (2012).
24. S. J. Zhang, Y. Li, Z. P. Liu, J. L. Ren, Y. F. Xiao, H. Yang, and Q. H. Gong, Appl. Phys. Lett. **105**, 061101 (2014).
25. S. Y. Ji, L. Yang, Y. L. Hu, J. C. Ni, W. Q. Du, J. W. Li, G. Zhao, D. Wu, and J. R. Chu, Small **13**, 1701190 (2017).
26. J. Lee, Y. Arita, S. Toyoshima, K. Miyamoto, P. Panagiotopoulos, E. M. Wright, K. Dholakia, and T. Omatsu, ACS Photonics **5**, 4156 (2018).